Pergamon

PII: S0097-8485(96)00033-2

Computers Chem. Vol. 21, No. 3, pp. 129–142, 1997

0097-8485/97 $17.00 + 0.00

Modeling and analysis of experimental atomic force microscope images of hard colloidal particles

Adam W. Marczewski* and Ko Higashitani
Department of Chemical Engineering, Kyoto University, Sakyo, Kyoto 606-01, Japan

(Received 18 June 1996; Accepted 7 November 1996)

Abstract—The fundamentals of atomic force microscopy (AFM) of hard colloidal particles are discussed. The idea of image modeling and deconvolution with the known AFM cantilever tip shape is described as well as a method for AFM tip calibration with the use of spherical colloidal particles. The algorithms and programs for AFM image modeling and experimental data analysis are presented together with exemplary analysis and possible applications. The difficulties of the method are discussed. Copyright © 1997 Elsevier Science Ltd. All rights reserved

Key words: atomic force microscopy, AFM, AFM tip calibration, AFM modeling

1. INTRODUCTION AND GENERAL CONSIDERATIONS

The atomic force microscope (AFM) is one of relatively new tools introduced into many branches of science (Griffith and Grigg, 1993). It belongs to a large family of microscope-like equipment where, instead of measurement of reflection or transmission of light or stream of electrons, other physical phenomena are utilized as a means of measuring certain microscopic properties of surfaces. Besides the AFM, the family includes: the scanning tunneling microscope (STM), the magnetic force microscope (MFM), the electrostatical force microscope (EFM) as well as various probe microscopes (e.g. the chemical probe microscope). In all of these instruments, a cantilever equipped with a suitable probe tip is moved over the sample surface. The appropriate physical effect is registered and subsequently analyzed. In the STM, the tunneling current between a metal cantilever tip and a conducting sample is measured, whereas in the AFM, MFM or EFM, the atomic, magnetic or electrostatic force is measured as a function of cantilever position. The chemical probe microscope is practically an AFM using cantilevers made of material displaying specific atomic interactions with various sample components or surface sites. Contrary to the well-known STM, the other instruments do not require the use of conducting sample and cantilever. There are also variants of AFM that can measure the orientation of atomic forces (the lateral force microscope, LFM, and friction force microscope, FFM). All of these devices create images by scanning sample surfaces in a linewise point-by-point manner. Recently, the so-called imaging AFM spectroscopy was introduced, where for every point of the image, the entire force curve (dependence force ~ distance) is analyzed (Baselt and Baldeschwieler, 1994).

Atomic force microscopy is a new method of investigating colloidal systems, making it possible to measure *in situ* the microscopic forces responsible for the specific colloidal behavior. Apart from the non-disputable value of such measurements, the basic features of colloids often make the interpretation of AFM data difficult or even—in certain cases—questionable. AFM was originally introduced, developed and is fully reliable and understood for relatively flat samples, whereas most colloidal systems contain spherical or elongated high aspect ratio particles and this simple fact should be taken into account.

With the AFM in its image-height mode, the micrometer-scale spring cantilever (usually equipped with a pyramid-shaped tip) is moved mechanically (typically by piezoelectric heads) over the sample surface (Fig. 1). The microscope analyzes the reflection of laser light from the polished cantilever end, determines its vertical position and moves the sample up or down in order to keep the force level (or cantilever deflection constant). In the case of relatively flat and chemically homogeneous samples, this results in keeping approximately constant the vertical distance between the tip apex and sample surface. The positions of the AFM tip are stored as a three-dimensional image of the sample. In the AFM force mode, the AFM measures the dependence of

*Corresponding author. Current address: Laboratory of Adsorption and Interface Physicochemistry, Institute of Catalysis and Surface Chemistry, Polish Academy of Sciences, M. Curie-Skłodowska Pl. 3, 20031 Lublin, Poland; E-mail awmaarcz@golem.umsc.lublin.pl; Fax: (+48)-81-5332811.

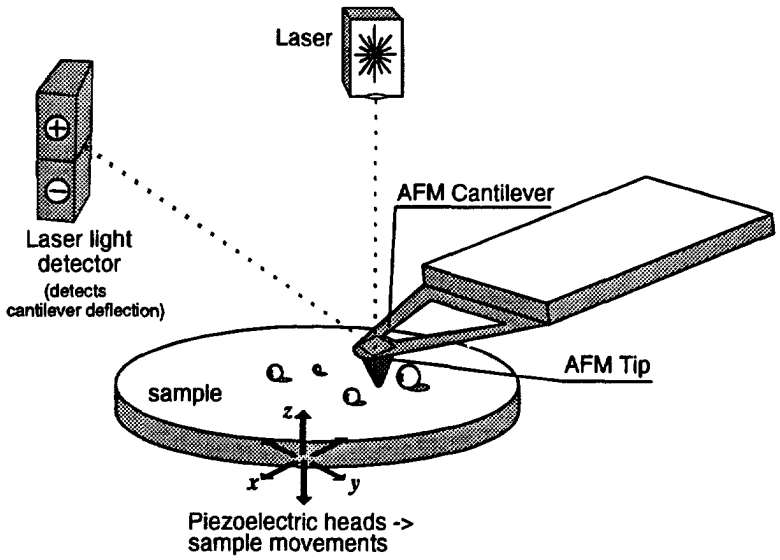

Fig. 1. A schematic drawing of the atomic force microscope.

force on the tip–sample distance in the following cycle: the tip is moved from "infinity" towards the sample; after reaching some maximum level of force "in contact", it is withdrawn back to the initial position ("infinity"). Other AFM modes are also known, but those described above are the most interesting ones in our case.

In order to describe the atomic interactions in the colloidal system one has to know exactly not only the chemical composition and topography of the system and surrounding media, but first of all the detailed geometry of its components. If all these data are known, the interaction between AFM tip and sample may be described generally through the simulation of forces between all the atoms present. In a simple system consisting of pure, regularly shaped solids placed in a vacuum, the main factor one should include are the dispersion forces (provided that the electrostatic forces may be neglected). Depending on the type of solids, other specific interactions may appear. In experiments conducted in the air or liquids, important factors are adsorption and adhesion. In electrolyte solutions both ionic and non-ionic solute adsorption and interactions play a very important role. Therefore AFM force data can be a valuable source of physicochemical data.

However, for modeling real systems, we encounter problems posed by the sample scale. Unfortunately, it is still difficult to include more than a few hundred atoms of the AFM tip-end (i.e. tip apex). Even for a very sharp tip, this represents just its rounded bottom part (with a radius 5–100 nm or more), while the tip shape a few nanometers above the tip apex is neglected. Thus the number of atoms involved in the simulation is limited to the small group of those close to the tip apex. This is just a fraction of the number of tip atoms that should be included in such calculations.

The limitation of the number of atoms that may be included in the simulation is the reason why the approach, while justified for relatively flat samples, seems to be quite inadequate when applied to such high aspect ratio samples as colloidal particles deposited on a flat surface (e.g. mica), or surfaces that are not perfectly level or horizontal. What happens when the tip approaches an object lying on a flat surface is a change of the point of contact from the tip apex to some point at the tip wall. This, obviously, is not taken into account by standard AFM interpretation programs (Fig. 2). For a worn-out, dull tip and small particles this change may be comparable to or even greater than the particle diameter (Allen *et al.*, 1992). However, for typical colloidal particles (e.g. with radius > 10 nm) in dry-air conditions, the differences in observed tip positions related to the differences in forces vs different spots on the tip, might be expected to be below 1 nm!

Thus, for typical colloidal systems the morphological (or simply geometrical) approach to atomic force microscopy (Markiewicz and Goh, 1994; Marczewski *et al.*, 1995a; Wilson *et al.*, 1995) should be favored. For such systems the tip geometry becomes the most important factor and interaction forces cannot be calculated without prior knowledge of the tip-shape data. This is mostly true for the "dry" colloidal systems, thus allowing the geometrical calibration (Markiewicz and Goh, 1994; Marczewski *et al.*, 1995a) of the AFM tip in favorable "dry" conditions. Afterwards, the calibration results may be used in the

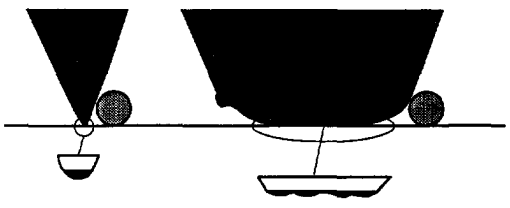

Fig. 2. Multiple points of contact between the AFM tip and colloidal sample for a real (blunt) tip vs an ideal (sharp) tip. Tip asymmetry, roughness and contamination are shown.

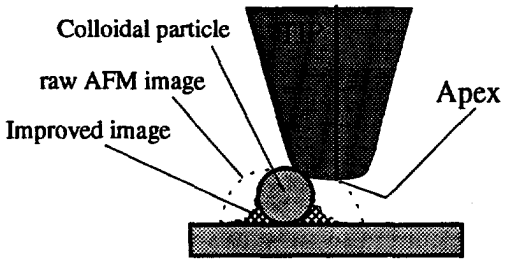

Fig. 3. The idea of AFM image modeling and deconvolution (improvement).

analysis of experiments in a "wet" environment, making it possible to improve the "force approach" by using the detailed geometrical definition of the tip.

2. MODELING AND DECONVOLUTION OF THE AFM IMAGES AND CALIBRATION OF THE AFM CANTILEVER TIP

The idea of modeling the AFM images of hard colloidal particles deposited on dry, flat solid surfaces or other hard high aspect ratio samples (Marczewski *et al.*, 1995a; Marczewski and Higashitani, 1995) is presented graphically in Fig. 3. The image recorded by the AFM program consists of the $[x, y, z]$ positions of the AFM tip apex vs coordinate origin $[xo, yo, zo]$. The true position of the tip apex may be determined up to the constant offset. The sample is usually moved by piezoelectric elements. Small vertical movements of the tip are detected with the help of a laser beam and photoelectric element, keeping it always (dynamically, through the feedback to sample movements) at a distance of an assumed force level between the tip and sample (Fig. 1). The cantilever structure should not allow lateral or angular tip movement so that all changes of photocurrent can be attributed to the changes of tip position, which is in turn due to the vertical component of the atomic force only.

While the sample is rigid (as e.g. a silica or titania particle on a mica support) and the cantilever force used in the measurement is large enough to make the distance between the tip and sample very small compared with the size of the sample features, then one can assume that the whole system can be referred to as one composed of classical rigid bodies. The possible error in determining tip–sample distance caused by this assumption should be almost constant (e.g. the distances plane–tip apex, and top-of-the-particle–tip apex are supposed to be almost the same). Thus the relative error ought to be negligible in comparison with the characteristic size of sample features.

Unfortunately, although this assumption is very reasonable for colloidal particles of size > 100 nm, it may lead to some image distortions in the case of much smaller particles.

2.1. AFM Image Modeling

When analyzing Fig. 3, one can see clearly that the AFM image of a spherical rigid particle should look like a small, usually asymmetrical, mountain. Because of purely steric reasons certain parts of the sample are never accessed by the tip. Whereas we assume that all the image points refer to the tip apex touching the sample surface, in the points of high curvature some other point of the tip can be in contact with the sample, thus leaving the apex hung over it. In this way, the sample image registered by the AFM is "falsified".

The image (height, or vertical apex position) is stored in $N \times N$ matrix **AFM**(i,j), where the lateral apex positions $[x(i), y(j)] = [x, y]$ vs a certain origin $[xo, yo]$ with constant lateral distance between image points given. If the surface shape is described by the $N \times N$ matrix **Surf**(i,j) and the AFM tip shape is defined as the $M \times M$ matrix **Tip**(i,j) (with the same spacing between points), then the algorithm for image creation is as follows (Fig. 4):

for all the surface points (i,j) (i.e. $[z(i,j), x(i), y(i)]$) place the tip image **Tip** with its apex-point (iax, jax) over the point (i,j) of the surface **Surf** and put it in such a vertical position that there is at least one tip point **Tip**(ip,jp) (and respective point of the sample surface **Surf**(iip,jjp)) where:

$$(\mathbf{Tip}(ip,jp) - \text{Apex}) + \mathbf{dz}(i,j) = \mathbf{Surf}(iip,jjp)$$

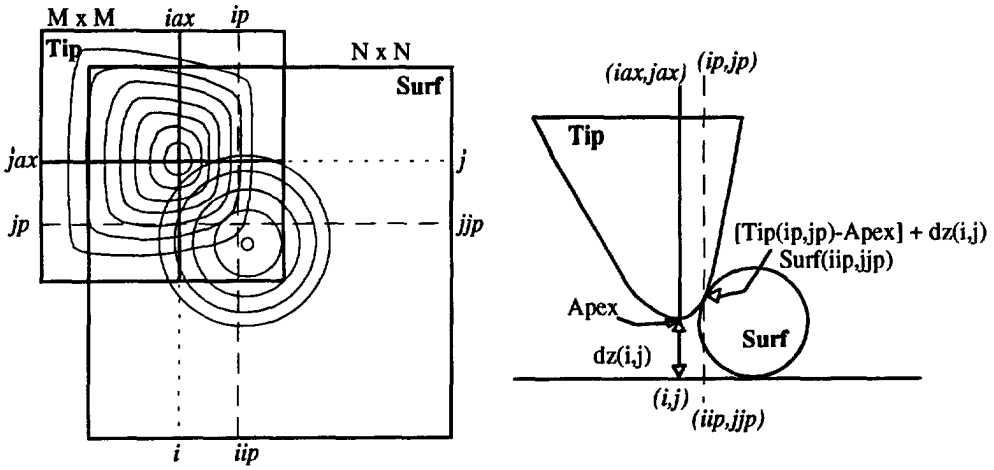

Fig. 4. A scheme of sample and tip-shape arrays, algorithm variables and their relations.

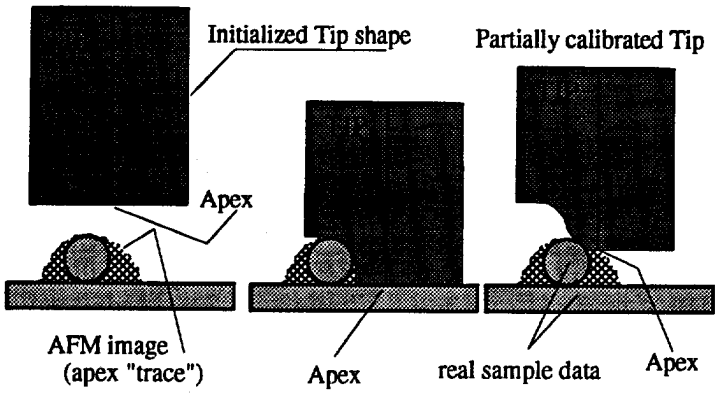

Fig. 5. The idea of AFM cantilever tip calibration (see text for explanations).

and all the points of the tip surface **Tip** are either above the sample surface **Surf** or are common for both:

$$(\mathbf{Tip}(ip,jp) - \text{Apex}) + \mathbf{dz}(i,j) \geq \mathbf{Surf}(iip,jjp)$$

where Apex is the vertical coordinate of the tip apex or the lowest point of the tip:

$$\min(\mathbf{Tip})_{ip,jp} = \mathbf{Tip}(iax,jax) \equiv \text{Apex}.$$

A simple algorithm to calculate $\mathbf{dz}(i,j)$ involves calculating the lowest point of the difference between the copy of the tip surface (with tip apex $\mathbf{Tip}(iax,jax)$ over point (i,j) of **Surf**) and the respective points of **Surf**. This value is equal to Apex $- \mathbf{dz}(i,j)$. Then, one gets the simulated AFM image:

$$\mathbf{AFM}(i,j) = \mathbf{Surf}(i,j) + \mathbf{dz}(i,j).$$

The matrix $\mathbf{dz}(i,j)$ contains the difference between the calculated (or experimental) AFM image and its assumed model (or true sample) surface. For a single-tipped cantilever we have $\mathbf{dz}(i,j) \geq 0$ and the highest values appear close to the steepest areas of the sample.

2.2. AFM Image Improvement/deconvolution

Similarly, when the AFM data are known from simulation or measurement, one can try to improve (or deconvolute) the data by using previously known tip data, **Tip**. The basic idea behind this is also very simple. The AFM image consists of an array of tip apex positions, though not necessarily apex–sample points-of-contact. Then, if we place the copy of the **Tip** array with its apex points defined by the respective AFM image points, part of the tip and AFM image may overlap (i.e. for a given image point $\mathbf{AFM}(i,j)$ we have $[\mathbf{Tip}(ip,jp) - \text{Apex}] + \mathbf{AFM}(i,j) < \mathbf{AFM}(iip,jjp)$ where (iip,jjp) is the AFM image point defined by the (ip,jp) point of the tip). We already know the AFM tip shape, so we must assume that part of the AFM image overlapping with the tip shape is not part of the sample and may be safely wiped away. Repeating this simple procedure for all AFM image points leads us to the deconvoluted image **Surfi** (Figs 4 and 5).

Nonetheless, one must remember that in most cases this deconvolution cannot be complete, because of the aforementioned steric hindrances. Though in some cases the improvement can be quite dramatic, e.g. for a blunt tip and small spherical particle, it may not be comparable with electron microscopy (EM) images—at least for "dry" systems.

2.3. Calibration of the AFM Cantilever Tip

Both simple procedures described above require the **Tip** matrix data to be known in advance.

The manufacturers of the atomic force microscopes and cantilevers supply the cantilever tip data with general information about tip material (e.g. Si_3N_4), tip shape (pyramid with specified opening angle, e.g. 18° or 35°), typical radius of the tip-end and cantilever tilt angle (18° for NanoScope II; 12° for NanoScope III). However, owing to some scatter in manufacturing results and also to the fact that the way the tip is mounted in the microscope may not be perfectly reproducible, these data are usually not reliable enough to be used in either of the procedures given above. Changes to the tip shape due to friction and sample-induced tip contamination during its longer usage are other important factors. Sadly, application of electron microscopy for tip imaging would entail additional costs and lead to some changes in the tip parameters that might render it non-usable afterwards.

Here, we may use a tip calibration procedure that requires merely the AFM itself, as well as a well-defined sample (Marczewski *et al.*, 1995a, 1995b). In general, the sample may be of any kind. However, we will consider a simple case of calibration—one that uses an easy to make and cheap sample consisting of hard spherical colloidal particles deposited on a flat support (e.g. mica plate). The sample need not be monodisperse—polydisperse spherical silica, titania or other commercially available colloids may be used.

In the process of tip calibration, the shape of a sample model for an isolated spherical particle deposited on a flat support is compared with its convoluted AFM image. This allows for the extraction of the tip shape.

In the initial stage of the procedure two matters are completed.

First, a geometrical model of the sample is created. This requires determining the particle support level and the position of the spherical particle top that defines both the particle diameter and position of its center. This is all the information we need to create

the sample model. For the sake of simplicity we assume that the term "tip apex" refers to its lowest point and that the cantilever is not double-tipped due to contamination or tip break-up, for instance.

Following this, we must assume a starting point for tip calibration, i.e. create a cube-shaped tip model larger than the real one (and often larger than the sample features) from which the procedure will "carve out" the true tip shape.

The proper calibration procedure is as follows (Figs 4 and 5):

> for all sample **Surf** and image **AFM** points (i,j) place the tip image over it with tip apex **Tip**(iax,jax) on point **AFM**(i,j); remove the part of tip that overlaps with sample model **Surf**.

This procedure is based on the assumption that both the sample model **Surf** and the sample image **AFM** are true, non-distorted data. As a logical consequence, the part of the tip image **Tip** that we initialized grossly as the cube, but which overlaps with the true, solid sample model, should be corrected. It yields the tip shape that is true up to the height slightly lower than the particle diameter (equal to its height for spherical particles). Even then, small inward features of the tip surface may or may not be revealed, depending on the particle curvature. (One may regard tip calibration as a procedure that is the reverse of AFM imaging, where the sample functions as a probe.) Data from several calibrations may be combined and the obtained tip shape may be extended higher by using the general information about tip shape, e.g. its opening angle and cantilever tilt angle.

The main advantage of this procedure is that it may be used repeatedly for any given tip with some reference sample. When used between experiments properly, it can constitute a simple tip-shape monitoring tool allowing for the control of tip wearing and contamination. One must, however, remember that the tip shape recovered from such a calibration is good up to the height less than the calibration particle diameter.

2.4. The *TipToe* Program

The authors developed a FORTRAN program *TipToe* for AFM image modeling and analysis of experimental AFM data as well as animated demonstration of creating model AFM images. All the following calculations have been performed with the aforementioned and other accessory programs.

The program consists of two main functional blocks: one for data modeling with the possibility of animated simulation of the AFM imaging process; the other for AFM experimental data analysis, correction and smoothing, and AFM tip calibration.

Simulations can be performed on sample surface arrays (32×32 to 1024×1024 elements) with a simulated plane or curved slope with deposited spherical, elliptical or round-ended rod-like particles or other shapes. The model tip (size from 15×15 to 511×511 elements) can be defined as cylindrical and paraboloidal (with the possibility of adding defects), or pyramid-like with a rounded end (defined through opening angle, cantilever tilt and twist angles, and tip-end radius). Noise and x, y, z-scale distortions may be simulated as well. Sample and tip arrays may have different x and y dimensions.

First, the AFM image is simulated (an animated presentation can be made), then using the assumed model and the simulated image the tip is calibrated and used to deconvolute (improve) the simulated image. The differences between the assumed and calculated shapes as well as the improvement of the AFM image are evaluated. All images can be analyzed as a two-dimensional projection bitmap image, cross-section profile or a three-dimensional image and saved on a disk as a 16- or 256-colors BMP file. All data arrays can be saved in text format.

The program reads and saves AFM height images in native NanoScope III format (short integer, i.e. 2B/point, data in binary file with text header). Although NanoScope III data are always 128×128, 256×256 or 512×512 in size, the accepted size range is the same as for data simulation. The original AFM data file is always protected against overwriting by the modified ones. Experimental AFM images can be: (i) smoothed/filtered or rescaled; (ii) improved (deconvoluted) with previously calibrated tip data; and (iii) for spherical particles only, used for tip calibration and data improvement (this can serve as an internal test of the calibration).

The difficult side of the simulation and calibration procedures described above involves memory and CPU time usage—memory required for storage of image data and working space alone is proportional to $N \times N$ (usually $N > M$) yielding for long integer or single precision real-image data (4B/point) from 0.5 MB for a 128×128 matrix to approximately 8 MB for a 512×512 data image (maximum for all arrays used). Currently however, such requirements are not excessive even for a typical Intel CPU-based PC: the program uses the simplified Windows 3.x memory model (MS Fortran 5.1 with QuickWin libraries) where the user has access to text-based and graphic windows (virtual or real size up to 1280×1024 pixels, 16 or 256 colors) and built-in memory management (up to 64 MB). Program *TipToe* was optimized to run even on 486/25 SX-based PCs with 4 MB RAM and 8 MB disk-swap file (though rather slowly for images larger than 128×128). To speed-up the program, almost all data manipulations are performed on long integer rather than real data, which allows it to run reasonably on machines without a numerical coprocessor. To optimize the memory access for large arrays most procedures were so arranged as to deal with 1 or 2 arrays at a time. A worse problem is the dependence of program run time on the product of AFM image array size and tip array size as time $\sim N \times N \times M \times M$. For a PC with an Intel Pentium-133/16 MB RAM (roughly comparable with Sun-SPARCstation 10 in execution speed) the execution time of one of the procedures (modeling, deconvolution or calibration) is of the order of approximately 30–40s for a 128×128 AFM image (the required size of the used Tip-shape data array is usually proportional to AFM data for typical surface aspect ratios—64×64 in this case) and grows 16 times for 256×256 ($\sim$ 600 s) and 256 times for 512×512 ($\sim$ 100 min) resolution images of the same sample

area, respectively (N^4 algorithm). Employing a faster processor or a 32-bit Fortran compiler instead of the 16-bit compiler can help. However, only the use of parallel processing can improve the situation markedly.

An Intel CPU-based PC was chosen as a platform of convenience because it can be run on the same PC that runs the AFM itself, thus alleviating problems with data transfer and the need for additional hardware. However, only the graphic part of the program is environment/system specific. The rest conforms to FORTRAN 77 with a few Microsoft extensions conforming to the Fortran 90 standard, and may be easily ported to other platforms.

3. RESULTS AND DISCUSSION

3.1. AFM Modeling

As an example, AFM image modeling, improvement and tip calibration were performed on a simulated low-resolution sample of 128 × 128 points (all other distance/size measurements are taken as relative to x, y data spacing). The AFM tip of the pyramidal shape (so-called tapping-mode tip in NanoScope, opening angle $\alpha = 35°$, tilt angle $\gamma = 12°$, tip-end radius $R = 30$) and sample consisting of a small spherical particle (radius $r = 10$) posted on a flat support were created—this is a case of the so-called blunt tip, or small particle ($r/R = 1/3$). An AFM image was simulated, then the tip calibration process was performed and subsequently image deconvoluted (improved). In Fig. 6 the assumed tip shape and the result of tip calibration are shown, whereas Figs 7 and 8 show simulated AFM images and results of image deconvolution, respectively. For greater emphasis, color bitmaps, image cross-sections and 3-D images are shown.

Not surprisingly, the result of tip calibration (Fig. 6) is very good almost up to the height (diameter) of the spherical particle used. However, above this tip area we have to extrapolate, use larger particles or use otherwise available general data about tip shape. The raw sample image (Fig. 7) shows that the image inherits its shape from both the spherical particle (e.g. height), as well as the AFM tip ("squarish" look, widened shape). A comparison of the raw sample image (Fig. 7) and deconvoluted image (Fig. 8) shows great improvement. The deconvolution is particularly efficient above half-height of the image. However, the lower part of the image still looks a little "squarish". The sample profiles allow us to compare a particle shape (sphere) and its image raw and deconvoluted.

3.2. Analysis of Experimental AFM Images

The experimental data discussed here have been measured with the NanoScope III Atomic Force Microscope (Digital Instruments, U.S.A.). Commercially available polydisperse spherical silica particles with diameters ranging from 50 to 500 nm (Nissan Kagaku Kogyo Co., Japan) have been used as samples. Particles were deposited on a mica plate by immersing them into a diluted, mildly ultrasonicated water suspension, and then drying. The concentration of the suspension was adjusted so as to avoid particle clustering.

Although the analysis of experimental images seems, conceptually, exactly the same as that of modeling particles, specific AFM-related errors make it quite different (Marczewski *et al.*, 1995b).

Model calculations (not shown here) indicate that there are some reasons for experimental image analysis and/or tip calibration to fail completely:

- erroneous scaling of x, y, z in the AFM image (e.g. due to nonlinearity and hysteresis of the piezoelectric scanners) (Snětivy and Vancso, 1993; Jørgensen *et al.*, 1994);
- AFM image noise with downward spikes results in an erosion of the deconvoluted sample. The lateral size of the erosion equals the size of the cross-section of the tip shape at that noise level (isolated upward noise spikes result in much smaller deconvolution errors or no error at all). Another effect of downward spikes is miscalibration of the tip of the same level (tip-end is sheared in this case);
- AFM scanline shifts make the image of a smooth sample look like that of a broken one. Accordingly the image of a spherical particle may be strongly distorted too; and
- when the sum of the tip-end and sample particle radii is large enough, the sample support is not level (flat) enough, and/or the image is noisy, then it is difficult to construct a reliable sample model, where the exact location of the particle top is required in order to perform the tip calibration.

In order to detect and correct erroneous instrument scaling, one has to use external standards (e.g. optical gratings are very good for x, y scale correction). This error may not be visible in the image appearance if the scale distortion is below a few percent. However, it may have a quite dramatic effect when the sample in question is intended as a calibration standard—both for the shape of the tip and for the deconvoluted images. These errors should be corrected (it can be done within the program *TipToe*) before any other operations are performed—especially if it is impossible to repeat the measurements for the given sample.

Several noise filtration methods are employed in the program: FFT filtering, wavelet (WT) filtering (Press *et al.*, 1992), several types of local smoothing methods (mean blur, Gaussian blur, two types of edge-preserving median filter) as well as the methods (developed by the authors) called "rolling" and "shaving". FFT filtering was found to be inadequate because the images analyzed are usually non-periodic in nature; however, WT filtering (removing lowest amplitude WT coefficients) proved to be quite adequate, allowing for the removal of high-frequency, low-magnitude noise without distorting the image features. Mean and Gaussian blur filters (size 3 × 3, 5 × 5 or 7 × 7) are used only when there is no other suitable method. Median filtering was found to be much more reliable, though. In "rolling" filtering, there are two elliptical "rolls" moved simultaneously over the top and bottom of the sample image surface. In its quick version, the average of the roll positions replaces the image. In its full, much slower version,

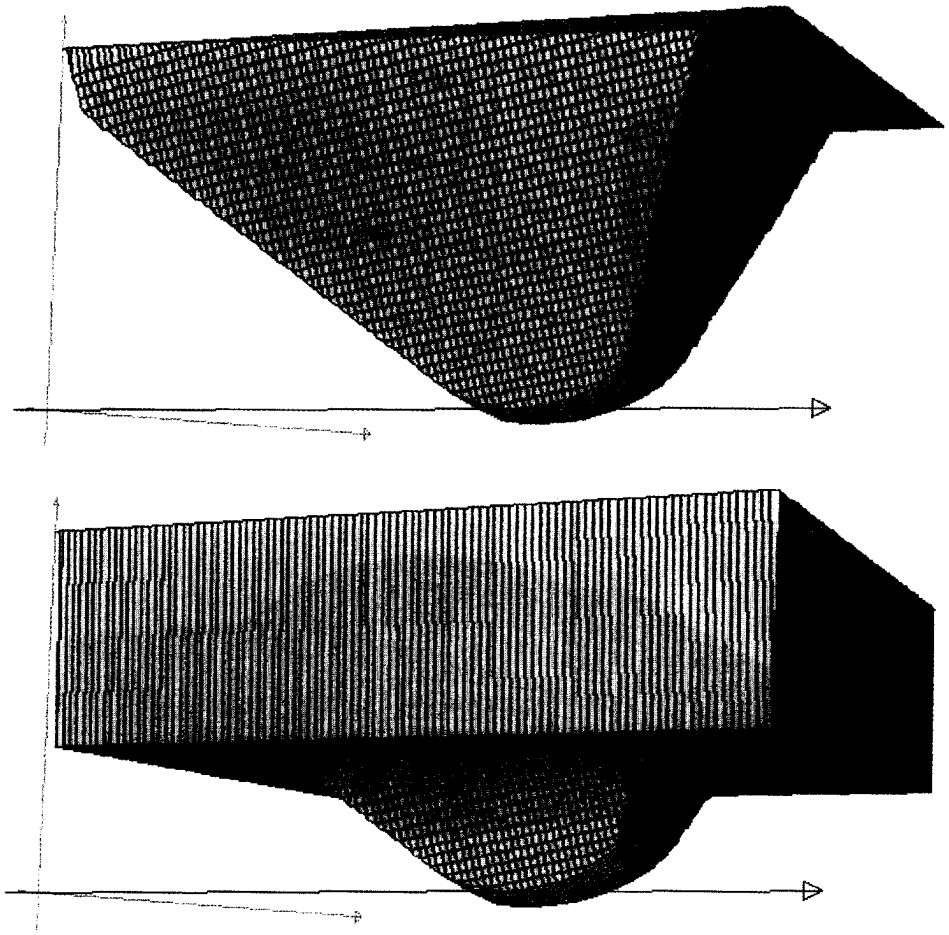

Fig. 6. Comparison of the assumed model tip and the result of tip calibration on a model sample (small colloidal particle) (simulated).

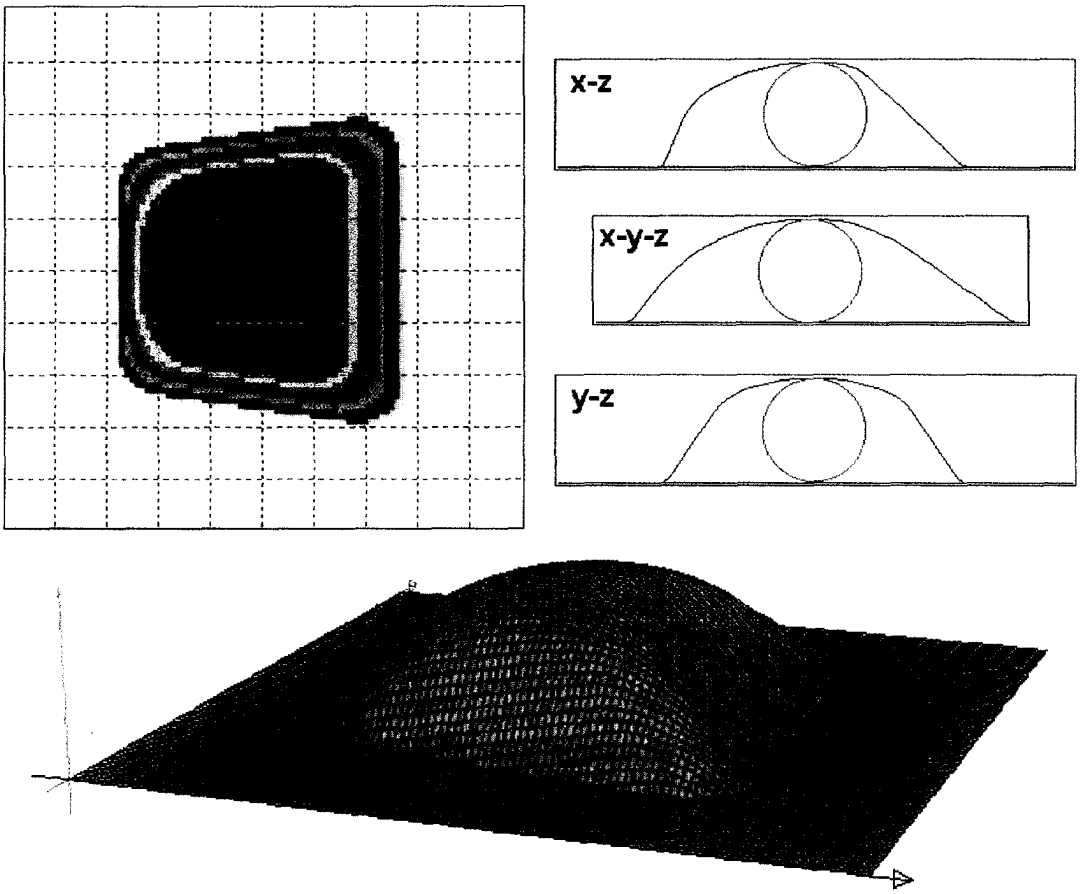

Fig. 7. A simulated AFM image of a small spherical particle for a blunt AFM tip (description in text).

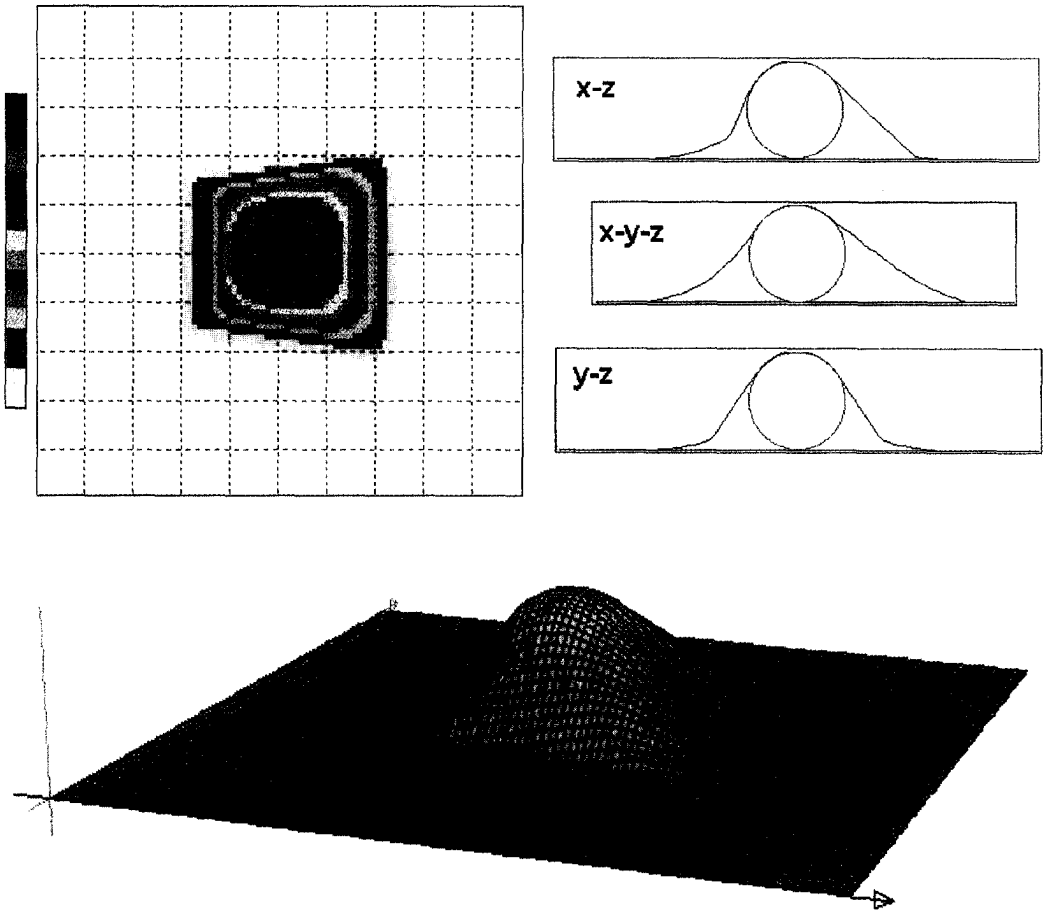

Fig. 8. A deconvoluted (improved) model AFM image (description in text).

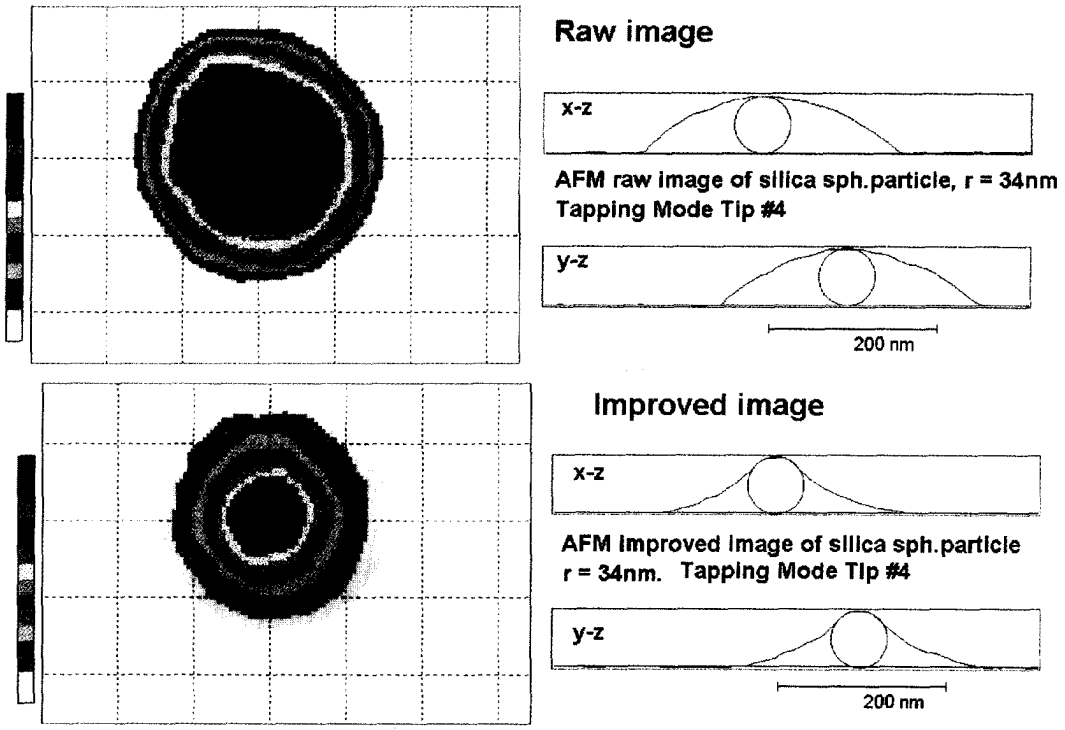

Fig. 9. Raw (top) and deconvoluted (bottom) experimental AFM images of a spherical silica particle (the estimated radius of the particle $r = 34$ nm; AFM tapping mode tip: the opening angle $\alpha \approx 18°$, the cantilever tilt angle $\gamma \approx 12°$).

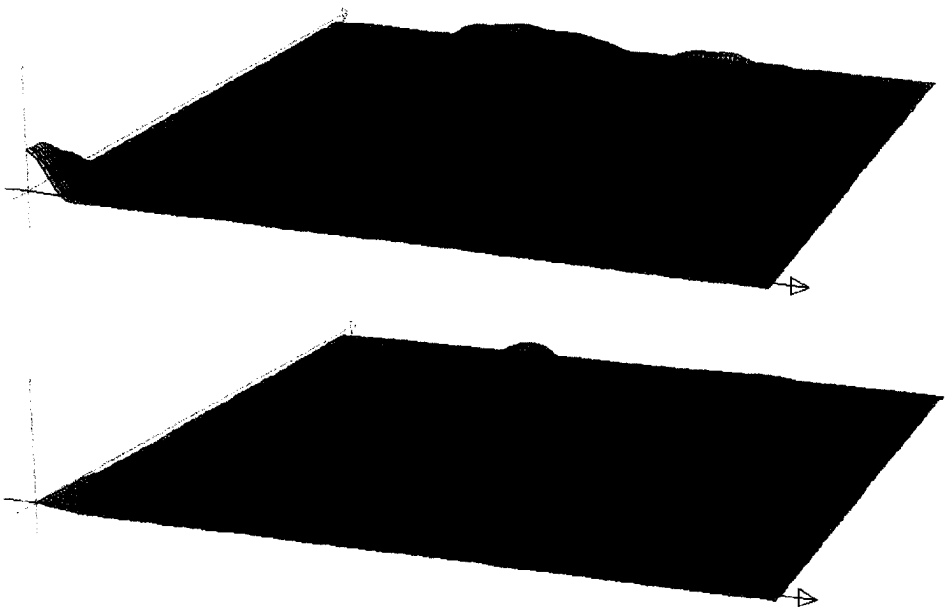

Fig. 10. Three-dimensional images of raw and deconvoluted sample images (compare with Fig. 9).

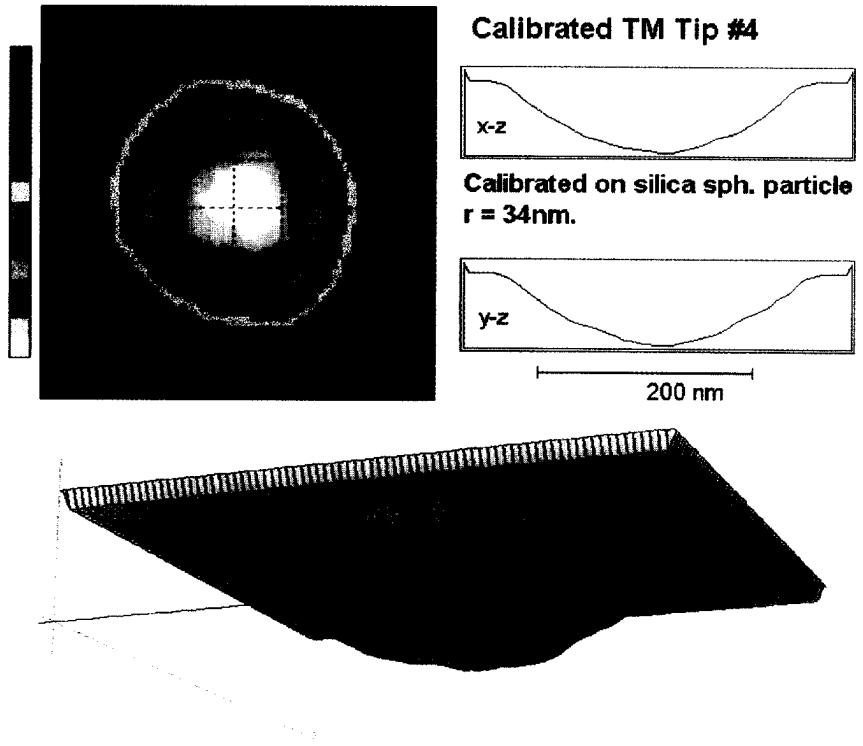

Fig. 11. The result of tip calibration on the sample shown in Figs 9 and 10. The estimated tip-end radius is ~ 200 nm (an old, worn-out tip was used).

rolls (one from the bottom, another one from the top) create their respective "fake" images (analogously to the aforementioned algorithms)—their average replaces the AFM image. In "shaving" filtering, two pairs of anti-symmetrical "rolls" and "shavers" are created. Each pair consists of a solid "roll" and a "shaver". The "roll" has an ellipsoidal bottom (for the upper pair) or ellipsoidal top (for the bottom one) with a vertical hole (or a scanline-aligned slit) of "infinite" depth. Each "shaver" is a copy of its respective "roll" with its hole (or slit) having finite depth (depending on the sample feature radius and noise level). The first "roll" is placed on the image surface, then replaced by the "shaver" and all points of the surface that are above its bottom (or below the top for the bottom pair) are cut out as noise. Again, the raw sample image is replaced by the combination of both results.

One may then have to correct possible scanline shifts (if there are any). First, the overall image slope has to be removed. If the sample is "empty-spaced" enough and not too noisy, one can pick some corner points and calculate the plane. When there is a noise problem, some parts of the image must be chosen (preferably those that look flat and do not contain eminent sample objects) and the sample plane (or some three-dimensional smooth surface) must be calculated through the LSQ approximation. After this the sample plane should be subtracted from the image. At this step, parts of the sample images apparently representing the sample support (e.g. mica plate) should be flat with their vertical coordinates (z) close to zero.

Here the so-called "scanline-flattening" procedure can be used. It is assumed that because of the nature of AFM measurement, separate scanlines can be shifted one versus another. Despite this, their shape, if not their vertical position, is generally maintained. Linear scanline-drift is also possible. The success of this procedure depends on finding areas of each of the scanlines, which can—and should—have the vertical coordinate 0, simply because they belong to the flat sample support. When such points (or areas) can be indicated to the procedure, they become reference points—separately calculated for each of the scanlines—through which the local drift line is "drawn", and then subtracted from all points of this scanline. Reference points will all assume 0 height value.

After smoothing the image the original slope can be safely restored—it may again be subtracted if required by the procedure involved, and restored afterwards.

Here one can already start image deconvolution with the known tip-shape array. Before this, the tip array, usually, must be rescaled. The reason is that tip calibration data are saved in the same resolution as that of the sample that was used for its calibration (though in native *TipToe*—not NanoScope—format), whereas every experimental data set is saved by NanoScope III as a short integer (2 byte) array with vertical and horizontal resolutions that are different for each sample. The corrected image can be compared with the raw image and saved in NanoScope III native format without overwriting the original.

When, however, our aim is to calibrate the cantilever tip, the next step is to create the sample model. When the particle is spherical (of unknown radius r) and the tip-end may also be approximated by a sphere (of unknown radius R), then the AFM image close to the top of the particle may be described as a sphere with radius equal to the sum $r + R$. This shape can also be approximated by the paraboloid $z(x,y)$:

$$z = 2r - \frac{1}{2(R+r)} \times [(x - x_c)^2 + (y - y_c)^2]$$

where the subscript "c" denotes the center of the spherical particle and $2r$ is the particle diameter and image height at the same time. This simple formula allows for easy LSQ determination of the particle diameter and position. However, the tip-end is usually flatter than the would-be sphere and the approximation itself is not precise enough and the sample image area where this approximation can be successfully used is usually quite narrow (e.g. points in the height range are above 90% of the particle height; in exceptional cases, for very small r/R ratio or very noisy data, one can use points above $\sim 50\%$ of particle height). The parameters of the paraboloid that we have obtained, permit a fast and rough estimation of the tip radius R. However, this approximation is sensitive to noise and changes in local curvature of the tip, which in turn rarely has a truly spherical end. On the other hand, tip-end radius can also be calculated from the shape of the AFM image "mountain" (height, width and approximate tip-opening angle and cantilever tilt angle).

After subtraction of the sample slope and scanline flattening, the level of particle support is $z = 0$ from definition and the sample model may be safely created: the sample slope is added to the plane ($z = 0$) with a sphere of radius r placed at (x_c,y_c) (see above).

At this stage one must create the tip model cube. The safest guess is the size of the image area where the height is greater than sample features' height. However, this is usually quite wasteful both in terms of storage and execution speed. The safe guess for the tip area is the size of the particle image (the details will not be discussed here). Then the calibration procedures described above can be used. Tip-shape array is saved in simple native *TipToe* format with text header and binary height data. The quality of calibration can be checked by deconvolution of the image used for calibration with this tip and comparison with the sample model sphere.

Figures 9 – 11 illustrate the results of applying *TipToe*, using the above-described procedures, to the analysis of a colloidal spherical silica particle sample. The quality of image improvement is similar to that attained for a simulated image. However, the surfaces of the sample and tip are not very smooth. In part this is due to experimental noise. The supposedly sharp ($R \sim 20$ nm) "tapping mode" tip has a distinct, blunt end, which is the result of prolonged use (many researchers interviewed by us admitted that they do not think about this effect too much, suspecting rather that tip contamination or instrument failure is the actual source of "doubtful" results).

Analogous results are obtained for other sizes of particles and AFM cantilever tips. One has to

caution, however, that for fresh, sharp tips (sharpness here is a relative measure, depending on the ratio of particle and tip radii), the effect of image deconvolution (improvement) will be less pronounced, though tip calibration will be equally successful and these data may be applied elsewhere.

4. CONCLUSIONS

The atomic force microscope is a valuable tool for investigating colloidal systems, especially non-conductive samples and liquid media. The method we propose for AFM image analysis makes it possible to extract more detailed information about the system. The method of calibration of the AFM cantilever tip allows one to obtain tip-shape data, which are essential in AFM image analysis and in physicochemical investigations (e.g. AFM force curve analysis). Image modeling increases the level of understanding of AFM imaging. The described program for image modeling, image analysis and AFM tip calibration can be used easily with typical PCs and AFM systems.

5. PROGRAM AVAILABILITY

Executable files (for MS Windows 3.x) and source files (Fortran) are available upon request.

REFERENCES

Allen, M. J., Hud, N. V., Balooch, M., Tench, R. J., Siekhaus, W. J. and Balhorn, R. (1992) *Ultramicroscopy* **42-44,** 1095.

Baselt, D. R. and Baldeschwieler, J. D. (1994) *Journal of Applied Physics* **76,** 33–38.

Griffith, J. E. and Grigg, D. A. (1993) *Journal of Applied Physics* **74,** 83–109.

Jørgensen, J. F., Carneiro, K., Madsen, L. L. and Conradsen, K. (1994) *Journal of Vacuum Science Technology Part B* **12,** 1702.

Marczewski, A. W., Yako, T. and Higashitani, K. (1995a) *Proceedings of the 60th Conference of the Society of Chemical Engineers*, Osaka, Japan, paper C108, Vol.I, p. 49. The Society of Chemical Engineers, Japan, Tokyo.

Marczewski, A. W., Yako, T. and Higashitani, K. (1995b) *Proceedings of the 48th Symposium of Colloidal and Surface Chemistry, Japanese Chemical Society*, Sapporo, Japan, paper P 015, p. 390. The Chemical Society of Japan, Tokyo.

Marczewski, A. W. and Higashitani, K. (1995) *Proceedings of the 48th Symposium of Colloidal and Surface Chemistry, Japanese Chemical Society*, Sapporo, Japan, paper 1C 05, p.154. The Chemical Society of Japan, Tokyo.

Markiewicz, P. and Goh, C. (1994) *Langmuir* **10,** 5.

Press, W. H., Teukolsky, S. A., Vetterling, W. T. and Flannery, B. P. (1992) *Numerical Recipes in FORTRAN*, 2nd ed. Cambridge University Press, Cambridge.

Snétivy, D. and Vancso, G. J. (1993) *Langmuir* **9,** 2253.

Wilson, D. L., Kump, K. S., Eppel, S. J. and Marchant, R. E. (1995) *Langmuir* **11,** 265.